Letter

Correlation between electronic and structural orders in 1*T*-$TiSe_2$

Hiroki Ueda,[1,*,§] Michael Porer,[1,*] José R. L. Mardegan,[1,†] Sergii Parchenko,[1,‡] Namrata Gurung,[2,3] Federica Fabrizi,[4] Mahesh Ramakrishnan,[1] Larissa Boie,[5] Martin Josef Neugebauer,[5] Bulat Burganov,[5] Max Burian,[1] Steven Lee Johnson,[5,6] Kai Rossnagel,[7,8] and Urs Staub[1,§]

[1]*Swiss Light Source, Paul Scherrer Institute, 5232 Villigen-PSI, Switzerland*
[2]*Laboratory for Multiscale Materials Experiments, Paul Scherrer Institute, 5232 Villigen-PSI, Switzerland*
[3]*Laboratory for Mesoscopic Systems, Department of Materials, ETH Zurich, 8093 Zurich, Switzerland*
[4]*Diamond Light Source Ltd., Diamond House, Harwell Science & Innovation Campus, Didcot, Oxfordshire OX11 0DE, United Kingdom*
[5]*Institute for Quantum Electronics, Physics Department, ETH Zurich, 8093 Zurich, Switzerland*
[6]*Laboratory for Non-linear Optics, Paul Scherrer Institute, 5232 Villigen-PSI, Switzerland*
[7]*Institut für Experimentelle und Angewandte Physik, Christian-Albrechts-Universität zu Kiel, 24098 Kiel, Germany*
[8]*Ruprecht-Haensel-Labor, Deutsches Elektronen-Synchrotron DESY, 22607 Hamburg, Germany*

(Received 17 June 2020; revised 19 February 2021; accepted 8 March 2021; published 5 April 2021)

The correlation between electronic and crystal structures of 1*T*-$TiSe_2$ in the charge-density wave (CDW) state is studied by x-ray diffraction in order to clarify basic properties in the CDW state, transport properties, and chirality. Three families of reflections are used to probe atomic displacements and the orbital asymmetry in Se. Two distinct onset temperatures are found: T_{CDW} and a lower T^* indicative for an onset of Se out-of-plane atomic displacements. T^* coincides with a DC resistivity maximum and the onset of the proposed gyrotropic (chiral) electronic structure. However, no indication for chirality is found. The relation between the atomic displacements and the transport properties is discussed in terms of Ti 3*d* and Se 4*p* states that only weakly couple to the CDW order.

DOI: 10.1103/PhysRevResearch.3.L022003

Electron (hole) localizations are central concepts in condensed matter systems and are directly relevant for charge-density wave (CDW) order, exciton formation, and superconductivity. The transition-metal dichalcogenide 1*T*-$TiSe_2$ has long been studied due to its wide variety of exciting physical phenomena such as CDW formation [1,2], the possible emergence of a Bose-Einstein exciton condensate [3,4], and, very recently, the observation of a gyrotropic electronic order [5]. Additionally, emergent superconductivity is found in the vicinity of the CDW phase [6–10]. This wide variety of properties suggests complex relations among electronic structure, transport, and the crystal structure [1,11–17]. Many of these basic properties are only poorly understood despite decades of intensive research on this material. Open points are (1) interplay of electronic and crystal structures below the CDW phase transition temperature T_{CDW} (≈202 K) and the DC resistivity maxima [1,17], and (2) a possible emergence of chirality in the crystal structure [18–20] or solely in the electronic structure [5,21–25], and its decoupling from the CDW (different onset temperature).

DC resistivity shows an increase at T_{CDW} which is due to charge localization and gap formation, similar to other CDW systems [26–28]. However, a large and broad peak in the resistivity is seen at a temperature lower than T_{CDW} [$T^* \approx 165$ K; see Ref. [1]]. It has been suggested that this anomalous peak originates from a crossover between two temperature regimes: from the low-temperature state with negative carriers (electrons) resulting from a small extrinsic doping to a high-temperature state with both negative and positive carriers (electrons and holes) which arise due to thermal fluctuations [17].

Besides the anomalous resistivity peak, the CDW state also features a circular photogalvanic current, measured with midinfrared circularly polarized light irradiation, interpreted as the occurrence of gyrotropic electronic order [5] and the emergence of chirality [18], both of which have distinct onset temperatures below T_{CDW}. The chiral phase transition, as claimed to be observed by scanning tunneling microscopy (STM) and x-ray diffraction (XRD) experiments [18–20], takes place ≈7 K lower than T_{CDW} [20]. Such a chiral CDW order is proposed as stacking three one-dimensional CDW layers with different wave vectors to each other in a chiral way [21–25], and is manifested by chiral atomic displacements with *P*1 symmetry and a possible orbital order. However, these experimental findings have been challenged by alternative

*These authors contributed equally to this work.
†Present address: Deutsches Elektronen-Synchrotron DESY, 22603 Hamburg, Germany.
‡Present address: Laboratory for Mesoscopic Systems, Department of Materials, ETH Zurich, 8093 Zurich, Switzerland.
§Corresponding authors: hiroki.ueda@psi.ch; urs.staub@psi.ch

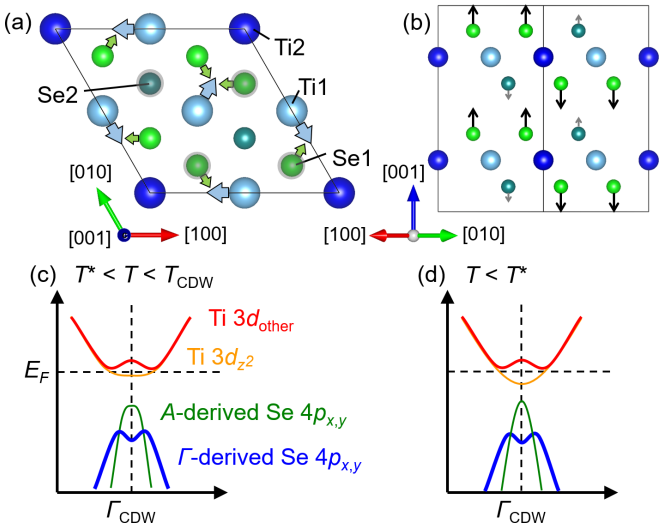

FIG. 1. Crystal structure of $1T$-$TiSe_2$ in the CDW state viewed along (a) [001] and (b) [110] (drawn by VESTA [43]). Arrows indicate the displacement directions from the normal state. Gray circles in (a) show Se in the lower layer with respect to the adjacent Ti layer. Schematic band structures of $1T$-$TiSe_2$ at (c) $T^* < T < T_{CDW}$ and (d) $T < T^*$. Panel (d) is similar to a sketch shown in Ref. [35]. T_{CDW} and T^* denote the CDW transition temperature and the onset temperature of reflections of family B (see text), respectively.

interpretations [29–31]. It is, therefore, important to clarify the electronic and crystal structures and their temperature dependence.

In this Letter, we study in detail the various structural modifications below T_{CDW} in a thin flake of single-crystalline $1T$-$TiSe_2$. The Bragg reflections, which appear in the CDW state, are ascribed to specific atomic motions. The change in transport properties below T_{CDW} is discussed in terms of a possible change of orbital hybridization caused by one of these atomic motions which weakly correlates to the CDW order. Although the onset temperature of certain reflections deviates from T_{CDW}, no evidence of chirality [20] is found. Detailed investigations of a space-group forbidden reflection in resonant XRD combined with *ab initio* simulation are well described by a nonchiral symmetry of electronic and crystal structures in the CDW state.

In the normal state above T_{CDW}, the $1T$-$TiSe_2$ crystal structure can be well described by space group $P\bar{3}m1$ [32]. It is a semiconductor with the Se $4p$ valence-band maximum lying at the Γ point and the Ti $3d$ conduction-band minima at the L points [see Fig. S1(a) of the Supplemental Material [33,34]]. The CDW order is represented by three wave vectors: $\mathbf{q}$ [$= \mathbf{a}^*/2 + \mathbf{c}^*/2$, $-\mathbf{b}^*/2 + \mathbf{c}^*/2$, and $-\mathbf{a}^*/2 + \mathbf{b}^*/2 + \mathbf{c}^*/2$, where $\mathbf{a}$, $\mathbf{b}$ and $\mathbf{c}$ are hexagonal bases used in Figs. 1(a) and 1(b)], which connect the Γ point and the L points as seen in Fig. S1(b) [33]. The formation of the triple-q CDW state results in a doubling of the hexagonal lattice parameters. The $2\times2\times2$ commensurate superlattice structure in the CDW state is well described by space group $P\bar{3}c1$ and is shown in Figs. 1(a) and 1(b). As a result of the CDW order, band folding occurs and all of the Γ, M, A, and L points in the normal state become the high-symmetric Γ_{CDW} point in the CDW state. Moreover, the valence-band maximum at the Γ point and the conduction-band minima (normal state L points) are strongly hybridized at the Γ_{CDW} point and are significantly repelled from the Fermi energy. A recent photoemission study revealed, however, that a branch of the conduction band derived from Ti $3d_{z^2}$ states remains as in the normal state, indicating only a weak correlation to the CDW order [35]. This Ti $3d_{z^2}$ band crosses the Fermi level and dominates transport properties in the CDW state. In contrast, the repulsion of the valence band maximum results in a valence-band maximum of the CDW state that is no longer at the Γ point but is located at the A point, at which the states are only weakly affected by the CDW order. The band structures for both the states are schematically drawn in Figs. S1(a) and 1(d) [33].

Both Ti and Se atoms, each of which occupies a single crystallographic site in the normal state ($P\bar{3}m1$), become two distinct sites in the CDW state ($P\bar{3}c1$), as shown in Figs. 1(a) and 1(b) [32]. While Ti1 and Se2 have only single in-plane (δ_{Ti}) or out-of-plane (δ_{Se2_out}) displacements from the normal state, respectively, Se1 has both types of components (δ_{Se1_in} and δ_{Se1_out} in-plane and out-of-plane, respectively). Since there are two Se sites, the out-of-plane motions of these sites are independent and we can define their difference as $\Delta z_{Se} = \delta_{Se1\_out} - \delta_{Se2\_out}$.

A single crystal of $1T$-$TiSe_2$ grown by the iodine vapor transport method [35] was cleaved along the (001) plane by repetitive exfoliation, and a flake (≈2 μm thickness) was mounted on a polycrystalline diamond substrate. Experiments were performed at the beamline I16 [36] of Diamond Light Source. The sample was mounted on the cold finger of a closed-cycle refrigerator attached to a Newport six-circle kappa diffractometer and cooled down well below T_{CDW} and T^*. The photon energies of x-ray beams were tuned to 12.6 keV for nonresonant XRD and around the Se K edge (≈12.658 keV) for resonant XRD. A Si (111) analyzer was used to determine the polarization state of the scattered beam. Scattered photons were counted using a PILATUS 100K pixel detector [37] and using an avalanche photodiode during azimuthal scans at resonance. A rocking curve as well as a raw two-dimensional image of (1 0 7) shown in Fig. S2 [33] confirm the high crystalline quality of the sample. An x-ray-absorption spectrum (XAS) was obtained by integrating the fluorescence signal. DC resistivity was measured for a single crystal from the same batch as that used for this XRD study along the (001) plane by the four-point resistance method. The resistivity peak at T^* of our sample is significant as seen in Fig. 2(a), and T^* matches that of a high-quality polycrystalline sample [1].

We classify the measured Bragg reflections into three families, A, B, and C, all of which are space-group forbidden in the normal state. We denote reflections by using the indices in the normal state, h, k, and l. Family A represents (h k l) reflections where l and at least one of h or k are half integers. These reflections appear at $\mathbf{G} + \mathbf{q}$, where $\mathbf{G}$ is a reciprocal-lattice vector of the normal state, and thus directly measure the displacement of the lattice from the CDW order. Family B represents the (0 k l) type of reflections where l is an integer while k is a half integer. Family C also represents the (0 k l) type of reflections but with both l and k as half integers. Note that family C is even space-group forbidden in

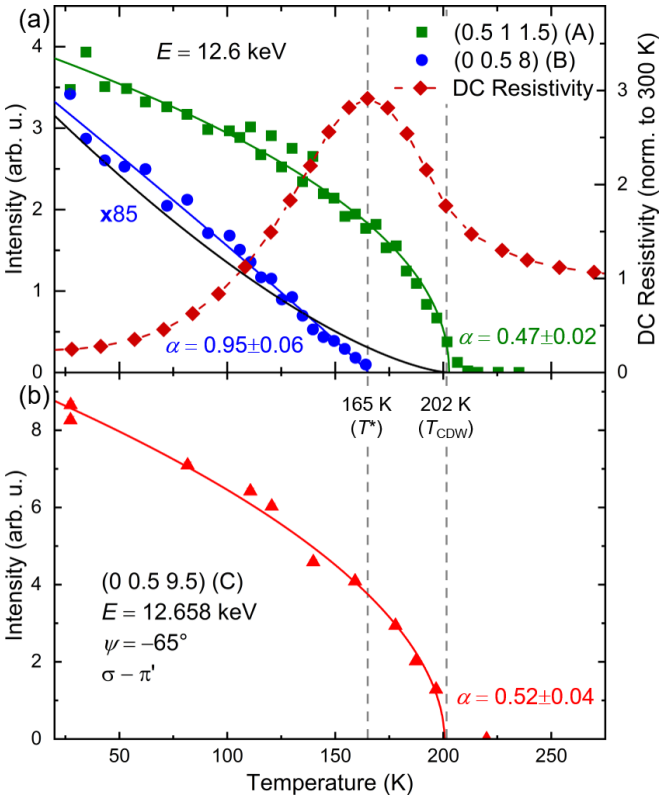

FIG. 2. Integrated intensities of reflections belonging to families A (0.5 1 1.5), B (0 0.5 8), and C (0 0.5 9.5), and DC resistivity as functions of temperature. XRD data shown in (a) [(b)] were acquired at 12.6 keV [the Se K edge]. The DC resistivity is normalized by the data at 300 K. The green, red, and blue solid lines represent power-law fits [$\propto (T_c - T)^{\alpha}$], where T_c and α are the critical temperature and critical exponent, respectively. The black line represents the quartic term with an onset at T_{CDW}.

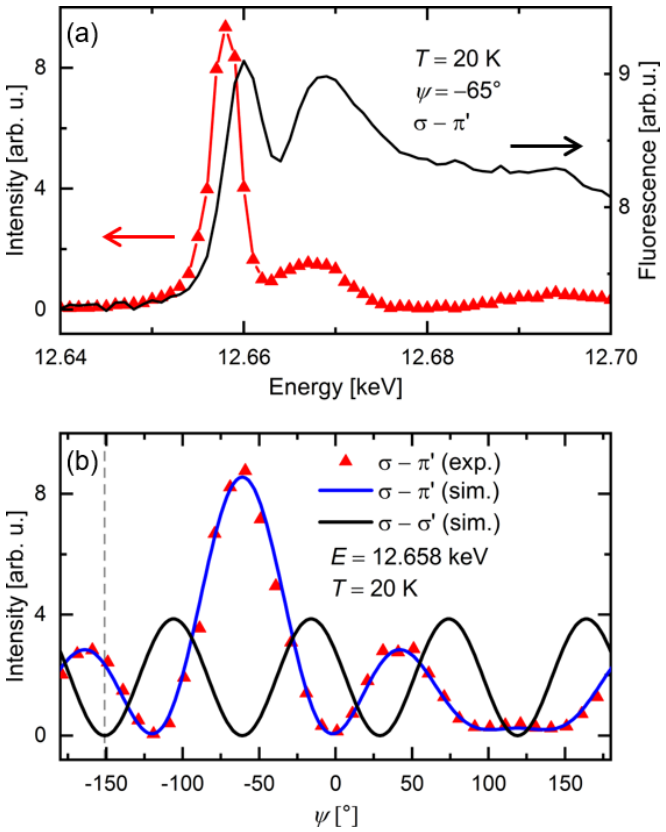

FIG. 3. (a) Photon-energy and (b) azimuthal-angle dependence of the (0 0.5 9.5). XAS (black line) is also shown in (a). Blue and black curves in (b) show the result of simulation using the FDMNES code [44]. Gray dotted line in (b) indicates the azimuthal angle where the data for Fig. S3 were taken.

the CDW state and is observed only at resonance (as shown later).

Figure 2 shows the temperature dependence of the integrated intensities of the three families together with the DC resistivity. The reflections (0.5 1 1.5) (family A, off resonance) and (0 0.5 9.5) (family C, at resonance) appear at T_{CDW} and their intensities grow proportional to the square root of T_{CDW}-T. Note that the temperature T_{CDW} is the same as that of a high-quality polycrystalline sample [1], indicating no significant impurity nor off-stoichiometry of our sample. On the other hand, the (0 0.5 8) (family B, off resonance) appears at T^*, which coincides with the DC resistivity maximum, and shows an approximately linear dependence with temperature (see Fig. S5 for further reflections [33]). These differences imply that A and B are sensitive to different atomic displacements allowed in the CDW state and that the displacements that dominate B have a correlation to the transport properties. The previously reported difference in the onset temperatures (≈7 K) of (1.5 1.5 0.5) and (2.5 1 0) [20] as well as the linear temperature dependence of (2.5 1 0) are reasonably explained by a fourth-order contribution of the *in-plane* CDW distortion occurring at T_{CDW} [31]. However, the observed difference in the onset temperatures (≈37 K) in our study cannot be explained in the same way since a calculated fourth-order contribution to the intensity [black curve in Fig. 2(a)] does not fit the experimentally obtained data for (0 0.5 8).

The (0 0.5 9.5) reflection, which is space-group forbidden in the CDW state, is observed only around the Se K edge as seen in Fig. 3(a). The intensity depends on the azimuthal angle, and the profile is nicely described by *ab initio* calculations performed by the FDMNES code using a model based on the crystal structure in the CDW state [32] [see Fig. 3(b)]. The polarization analysis at the specific azimuthal angle displayed in Fig. S3 is consistent with the calculated results where the reflection gives finite intensity in the σ–π' channel but no signal in the σ–σ' channel. On the basis of such profiles, which are well reproduced by our *ab initio* calculations, and the symmetry analyses (see the Supplemental Material of [33]), the (0 0.5 9.5) space-group forbidden reflection intensity is explained by an aspheric electron distribution in the Se1 orbitals in the CDW state, also often called ATS (anisotropic tensor susceptibility) scattering [38].

The x-ray absorption at the Se K edge includes the excitation of an electron from the 1s state to the 4p valence state, which would be totally occupied in a fully ionic picture. Thus, the observation of the space-group forbidden reflection means that there are holes in the Se valence state in addition to the aspheric electron distribution in the Se1 4p, as predicted in Ref. [39] by DFT calculations. It is obvious that the change

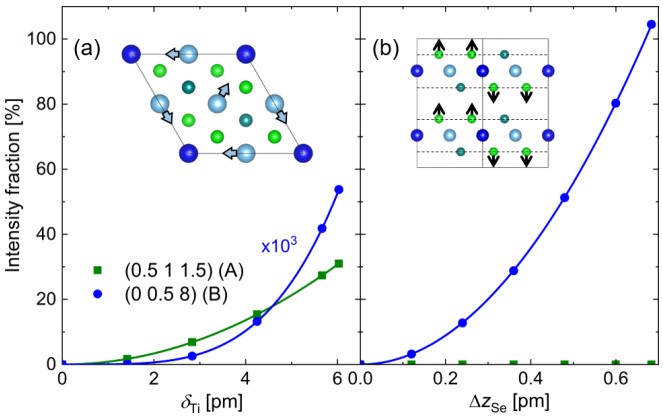

FIG. 4. Numerically calculated intensities of (0.5 1 1.5) (green) and (0 0.5 8) (blue) reflections as functions of (a) δ_{Ti} and (b) Δz_{Se}. The data are normalized by the intensity calculated for the reported structure in the CDW state [32]. The respective displacements are schematically displayed as insets. The green line in (a) and blue line in (b) represent a quadratic and the blue line in (a) a quartic function.

in orbital asphericity is associated with the CDW order since its onset temperature coincides with the appearance of reflections A. The absence of calculated intensities for artificially removed in-plane CDW distortions for the reflection further confirms this relation [33]. In addition, the anisotropic environment of the hybridized Ti $3d$ states, associated with the CDW structure, allows the formation of an excitonic state [3,4] generating holes in the Se $4p$ bands which influence the electron distribution of the Se.

To identify the nature of atomic displacements dominating space-group allowed reflections A and B, numerical calculations for possible models with different types of displacements were carried out and are summarized in Table S2 of the Supplemental Material [33] (see Ref. [33] for details of the models and procedure). We find that δ_{Ti} and δ_{Se1_in}, both in-plane displacements, dominate A while Δz_{Se}, relating to an out-of-plane displacement, dominates B. Figure 4 shows the calculated intensities of the (0.5 1 1.5) and (0 0.5 8) reflections as function of δ_{Ti} and Δz_{Se} [the dependence on δ_{Se1_in} shows a similar behaviors to that of δ_{Ti}, which is shown in Fig. S6(a) [33]]. A is largely dominated by δ_{Ti} through a quadratic contribution to the intensity (linear in the structure factor) without any contribution from Δz_{Se}. On the other hand, B is dominated by Δz_{Se} ($\propto \Delta z_{Se}{}^2$) with a 10^3 times smaller quartic contribution in δ_{Ti}. The quartic contribution of δ_{Ti} to the intensity can explain the linear temperature dependence of B but cannot explain the significant intensity and the difference in onset temperature from A. Thus, it is plausible that Δz_{Se} sets in $\approx$37 K lower than T_{CDW} and develops slower as a function of temperature while cooling than the CDW order parameters reflected by δ_{Ti} and δ_{Se1_in}. These observations are possible when Δz_{Se} is not the primary order parameter of the CDW phase transition. The difference in onset temperatures between (1.5 1.5 0.5) and (2.5 1 0) reported earlier [20,31] are not related to our observations since (2.5 1 0) is independent of Δz_{Se} (as $l = 0$). As shown in Ref. [31], the temperature dependence of (2.5 1 0) is naturally explained by the quartic behavior of the in-plane displacements. However, the anomaly in the specific heat found in that study [20] might be directly related to Δz_{Se}.

Whereas the CDW order largely affects the band structure, the maximum of the DC resistivity is not correlated to T_{CDW} but T^*, around which the gyrotropic electronic order also appears [5]. Note that T_{CDW} can vary between different samples, probably due to differences in defect density [1]. The displacements δ_{Ti} and δ_{Se1_in} dominate the CDW distortion and Δz_{Se} does not further break the symmetry in the CDW state. The Δz_{Se}, the magnitude of which is much smaller than δ_{Ti} and δ_{Se1_in}, creates only a tiny change in the structure of the main bands that form the hybridization gap. The onset of δ_{Se1_in} shortens the Se1-Ti bond length compared to Se2-Ti, and Se1 moves away from the adjacent Ti layer below T^*. This could weaken the orbital hybridization between Ti $3d_{z2}$ and Se $4p_{x,y}$ at the A point, increasing the band curvatures of the specific branches [compare Figs. 1(c) and 1(d)]. Therefore, the carriers in Ti $3d_{z2}$ and A-derived Se $4p_{x,y}$ would acquire lighter effective masses and longer mean free paths, resulting in a decrease of DC resistivity below T^*. Note that the Ti $3d_{z2}$, which crosses the Fermi energy, dominates the transport in the CDW state. Carriers due to thermal fluctuations could additionally contribute to the transport [17].

Interestingly, for both Cu_xTiSe_2 ($x = 0.05$) and $1T$-$TiSe_2$ at $\geqslant$2.82 GPa, the anomalous peak in the DC resistivity vanishes and a superconducting state appears upon lowering the temperature [6,7]. These samples have the same space group and CDW transition as $1T$-$TiSe_2$ under ambient pressures, but the distortion Δz_{Se} is zero in the CDW state for both the doped and pressurized samples [32]. This implies that Δz_{Se} plays a critical role in the transport properties and might be a key parameter governing the emergence of the superconducting state.

We now comment on the possible occurrence of chirality in the CDW state. Even though the B reflections have a lower onset temperature than T_{CDW}, a symmetry analysis based on the Landau theory valid for this second order phase transition is inconsistent with the occurrence of chirality [5]. The circular photogalvanic current, which is claimed as the evidence for a chiral electronic structure, appears at almost the same temperature as the structural modification [5]. This suggests that a possible chirality in the electronic states would be significantly coupled to the lattice, and therefore the underlying crystal lattice should be chiral. Observation of orbital asphericity through studying the polarization dependence of space-group forbidden reflections in resonant XRD is one of the established methods to determine the presence of chirality in crystal lattices and in orbital structures [40–42]. However, the observed polarization-dependent azimuthal-angle dependence of the (0 0.5 9.5) reflection is very well reproduced by the *ab initio* calculations assuming the nonchiral space group $P\bar{3}c1$. Moreover, if the space group is $P1$ as claimed in earlier studies as a "chiral" space group [21–25], this reflection must be a symmetry allowed reflection. The absence of an intensity for this reflection at off resonance and in the $\sigma-\sigma'$ channel is shown in Figs. 3(a) and 3(b), respectively. This indicates that the reflection is space-group forbidden, ruling out possible chiral space groups, as well as the proposed space group $P1$.

Therefore, we can conclude that our results give strong support for the absence of chirality of the Se orbitals (electronic and crystal structure) and speak against $P1$ symmetry (crystal structure) in the CDW state.

In summary, we examined the charge-density wave (CDW) phase of $1T$-$TiSe_2$ by means of x-ray diffraction. One of the studied three families of reflections has different onset temperature compared to the others. Our detailed analysis revealed that the family of reflections comes from the difference in relative out-of-plane motion between the two Se sites, which weakly couples to the CDW order. The different onset temperature compared to the CDW transition of the reflection is not caused by the onset of chirality, and chirality in the CDW state is not found in the crystal structure or in the Se orbital pattern. The out-of-plane atomic displacements of Se can reduce the orbital hybridization between Ti $3d_{z2}$ and Se $4p_{x,y}$ states, which couple only weakly to the CDW order. The consequent decrease of the effective mass of carriers results in a reduction of DC resistivity at lower temperatures. Our x-ray-diffraction results provide the crucial link between the origin of the anomalous feature in transport properties and structural modifications that change the hybridization in the relevant electronic bands. This specific picture clarifies now the microscopic origin of the transport properties of $1T$-$TiSe_2$. Experimental and model data are accessible from the Materials Cloud Archive [45].

We thank C. Monney and T. Jaouen for enlightening discussions. The x-ray-diffraction experiments were performed at the beamline I16 (Diamond Light Source) and the X04SA beamline (Swiss Light Source). This work was supported by Swiss National Science Foundation (Sinergia Project "Toroidal moments," Grant No. CRSII2_147606) and its National Centers of Competence in Research, NCCR MUST Grant No. 51NF40-183615 and NCCR MARVEL. The research leading to this result has also been supported by the project CALIPSOplus under Grant Agreement No. 730872 from the EU Framework Programme for Research and Innovation HORIZON 2020 and H.U. acknowledges financial support from Horizon 2020, the EU Framework Programme for Research and Innovation under the Marie Skłodowska-Curie Grant Agreement No. 801459-FP-RESOMUS.

[1] F. J. Di Salvo, D. E. Moncton, and J. V. Waszczak, Electronic properties and superlattice formation in the semimetal $TiSe_2$, Phys. Rev. B **14**, 4321 (1976).

[2] L. J. Li, E. C. T. O'Farrell, K. P. Loh, G. Eda, B. Özyilmaz, and A. H. Castro Neto, Controlling many-body states by the electric-field effect in a two-dimensional material, Nature (London) **529**, 185 (2016).

[3] H. Cercellier, C. Monney, F. Clerc, C. Battaglia, L. Despont, M. G. Garnier, H. Beck, P. Aebi, L. Patthey, H. Berger, and L. Forró, Evidence for an Excitonic Insulator Phase in $1T$-$TiSe_2$, Phys. Rev. Lett. **99**, 146403 (2007).

[4] A. Kogar, M. S. Rak, S. Vig, A. A. Husain, F. Flicker, Y. I. Joe, L. Venema, G. J. MacDougall, T. C. Chiang, E. Fradkin, J. van Wazel, and P. Abbamonte, Signatures of exciton condensation in a transition metal dichalcogenide, Science **358**, 1314 (2017).

[5] S.-Y. Xu, Q. Ma, A. Kogar, A. Zong, A. M. Mier Valdivia, T. H. Dinh, S.-M. Huang, B. Singh, C.-H. Hsu, T.-R. Chang, J. P. C. Ruff, K. Watanabe, T. Taniguchi, H. Lin, G. Karapetrov, D. Xiao, P. Jarillo-Herrero, and N. Gedik, Spontaneous gyrotropic electronic order in a transition-metal dichalcogenide, Nature (London) **578**, 545 (2020).

[6] E. Morosan, H. W. Zandbergen, B. S. Dennis, J. W. G. Bos, Y. Onose, T. Klimczuk, A. P. Ramirez, N. P. Ong, and R. J. Cava, Superconductivity in Cu_xTiSe_2, Nat. Phys. **2**, 544 (2006).

[7] A. F. Kusmartseva, B. Sipos, H. Berger, L. Forró, and E. Tutiš, Pressure Induced Superconductivity in Pristine $1T$-$TiSe_2$, Phys. Rev. Lett. **103**, 236401 (2009).

[8] M. Maschek, S. Rosenkranz, R. Hott, R. Heid, M. Merz, D. A. Zocco, A. H. Said, A. Alatas, G. Karapetrov, S. Zhu, J. van Wezel, and F. Weber, Superconductivity and hybrid soft modes in $TiSe_2$, Phys. Rev. B **94**, 214507 (2016).

[9] E. Morosan, K. E. Wagner, L. L. Zhao, Y. Hor, A. J. Williams, J. Tao, Y. Zhu, and R. J. Cava, Multiple electronic transitions and superconductivity in Pd_xTiSe_2, Phys. Rev. B **81**, 094524 (2010).

[10] H. Luo, W. Xie, J. Tao, I. Pletikosic, T. Valla, G. S. Sahasrabudhe, G. Osterhoudt, E. Sutton, K. S. Burch, E. M. Seibel, J. W. Krizan, Y. Zhu, and E. J. Cava, Differences in chemical doping matter: Superconductivity in $Ti_{1-x}Ta_xSe_2$ but not in $Ti_{1-x}Nb_xSe_2$, Chem. Mater. **28**, 1927 (2016).

[11] K. Rossnagel, L. Kipp, and M. Skibowski, Charge-density-wave phase transition in $1T$-$TiSe_2$: Excitonic insulator versus band-type Jahn-Teller mechanism, Phys. Rev. B **65**, 235101 (2002).

[12] C. Monney, H. Cercellier, C. Battaglia, E. F. Schwier, C. Didiot, M. G. Garnier, H. Beck, and P. Aebi, Temperature dependence of the excitonic insulator phase model in $1T$-$TiSe_2$, Physica B **404**, 3172 (2009).

[13] C. Monney, E. F. Schwier, M. G. Garnier, N. Mariotti, C. Didiot, H. Beck, P. Aebi, H. Cercellier, J. Marcus, C. Battaglia, H. Berger, and A. N. Titov, Temperature-dependent photoemission on $1T$-$TiSe_2$: Interpretation within the exciton condensate phase model, Phys. Rev. B **81**, 155104 (2010).

[14] C. Monney, E. F. Schwier, M. G. Garnier, N. Mariotti, C. Didiot, H. Cercellier, J. Marcus, H. Berger, A. N. Titov, H. Beck, and P. Aebi, Probing the exciton condensate phase in $1T$-$TiSe_2$ with photoemission, New J. Phys. **12**, 125019 (2010).

[15] S. Koley, M. S. Laad, N. S. Vidhyadhiraja, and A. Taraphder, Preformed excitons, orbital selectivity, and charge density wave order in $1T$-$TiSe_2$, Phys. Rev. B **90**, 115146 (2014).

[16] B. Hildebrand, T. Jaouen, C. Didiot, E. Razzoli, G. Monney, M.-L. Mottas, A. Ubaldini, H. Berger, C. Barreteau, H. Beck, D. R. Bowler, and P. Aebi, Short-range phase coherence and origin of the $1T$-$TiSe_2$ charge density wave, Phys. Rev. B **93**, 125140 (2016).

[17] M. D. Watson, A. M. Beales, and P. D. C. King, On the origin of the anomalous peak in the resistivity of $TiSe_2$, Phys. Rev. B **99**, 195142 (2019).

[18] J. Ishioka, Y. H. Liu, K. Shimatake, T. Kurosawa, K. Ichimura, Y. Toda, M. Oda, and S. Tanda, Chiral Charge-Density Waves, Phys. Rev. Lett. **105**, 176401 (2010).

[19] J. Ishioka, T. Fujii, K. Katono, K. Ichimura, T. Kurosawa, M. Oda, and S. Tanda, Charge-parity symmetry observed through Friedel oscillations in chiral charge-density waves, Phys. Rev. B **84**, 245125 (2011).

[20] J. Castellan, S. Rosenkranz, R. Osborn, Q. Li, K. E. Gray, X. Luo, U. Welp, G. Karapetrov, J. P. C. Ruff, and J. Wezel, Chiral Phase Transition in Charge Ordered 1T-$TiSe_2$, Phys. Rev. Lett. **110**, 196404 (2013).

[21] J. van Wezel and P. Littlewood, Viewpoint: Chiral symmetry breaking and charge order, Physics **3**, 87 (2010).

[22] J. van Wezel, Chirality and orbital order in charge density waves, Eurphys. Lett. **96**, 67011 (2011).

[23] J. van Wezel, Prerequisites for chiral charge order, Physica B **407**, 1779 (2012).

[24] B. Zenker, H. Fehske, H. Beck, C. Monney, and A. R. Bishop, Chiral charge order in 1T-$TiSe_2$: Importance of lattice degrees of freedom, Phys. Rev. B **88**, 075138 (2013).

[25] J. van Wezel, Observing the chiral charge ordering transition in $TiSe_2$, Adv. Sci. Tech. **90**, 103 (2014).

[26] M. Sato, H. Fujishita, S. Sato, and S. Hoshino, Neutron inelastic scattering and x-ray structural study of the charge-density-wave state in $K_{0.3}MoO_3$, J. Phys. C: Solid State Phys. **18**, 2603 (1985).

[27] Z. Dian-lin, L. Shu-Yuan, B. J. Jin, and C. W. Chu, Simultaneous measurements of resistivity and thermopower of orthorhombic TaS_3 under pressure, Phys. Rev. B **37**, 4502 (1988).

[28] M. S. da Luz, A. de Campos, B. D. White, and J. J. Neumeier, Electrical resistivity, high-resolution thermal expansion, and heat capacity measurements of the charge-density wave compound γ-Mo_4O_{11}, Phys. Rev. B **79**, 233106 (2009).

[29] A. M. Novello, B. Hildebrand, A. Scarfato, C. Didot, G. Monney, A. Ubaldini, H. Berger, D. R. Bowler, P. Aebi, and Ch. Renner, Scanning tunneling microscopy of the charge density wave in 1T-$TiSe_2$ in the presence of single atom defects, Phys. Rev. B **92**, 081101(R) (2015).

[30] B. Hildebrand, T. Jaouen, M.-L. Mottas, G. Monney, C. Barreteau, E. Giannini, D. R. Bowler, and P. Aebi, Local Real-Space View of the Achiral 1T-$TiSe_2$ 2×2×2 Charge Density Wave, Phys. Rev. Lett. **120**, 136404 (2018).

[31] M.-K. Lin, J. A. Hlevyack, P. Chen, R.-Y. Liu, and T.-C. Chiang, Comment on "Chiral Phase Transition in Charge Ordered 1T-$TiSe_2$", Phys. Rev. Lett. **122**, 229701 (2019).

[32] S. Kitou, A. Nakano, S. Kobayashi, K. Sugawara, N. Katayama, N. Maejima, A. Machida, T. Watanuki, K. Ichimura, S. Tanda, T. Nakamura, and H. Sawa, Effect of Cu intercalation and pressure on excitonic interaction in 1T-$TiSe_2$, Phys. Rev. B **99**, 104109 (2019).

[33] See Supplemental Material at http://link.aps.org/supplemental/10.1103/PhysRevResearch.3.L022003 for more information of the sample quality, symmetry analyses, *ab initio* calculations, experimental results of further reflections, and the numerical calculations for diffraction intensities.

[34] A. Zunger and A. J. Freeman, Band structure and lattice instability of $TiSe_2$, Phys. Rev. B **17**, 1839 (1978).

[35] M. D. Watson, O. J. Clark, F. Mazzola, I. Marković, V. Sunko, T. K. Kim, K. Rossnagel, and P. D. C. King, Orbital- and k_z-Selective Hybridization of Se 4p and Ti 3d States in the Charge Density Wave Phase of $TiSe_2$, Phys. Rev. Lett. **122**, 076404 (2019).

[36] S. P. Collins, A. Bombardi, A. R. Marshall, J. H. Williams, G. Barlow, A. G. Day, M. R. Pearson, R. J. Woolliscroft, R. D. Walton, G. Beutier, and G. Nisbet, Diamond beamline I16 (Materials & Magnetism), in *SRI 2009, 10th International Conference on Radiation Instrumentation*, AIP Conf. Proc. No. 1234 (AIP, Melville, NY, 2010), pp. 303–306.

[37] Ch. Broennimann, E. F. Eikenberry, B. Hentich, R. Horisberger, G. Huelsen, E. Pohl, B. Schmitt, C. Schulze-Briese, M. Suzuki, T. Tomizaki, H. Toyokawa, and A. Wagner, The PILATUS 1M detector, J. Synchrotron Rad. **13**, 120 (2006).

[38] V. E. Dmitrienko, Forbidden reflections due to anisotropic x-ray susceptibility of crystals, Acta Cryst. A **39**, 29 (1983).

[39] M. Hellgren, J. Baima, R. Bianco, M. Calandra, F. Mauri, and L. Wirtz, Critical Role of the Exchange Interaction for the Electronic Structure and Charge-Density-Wave Formation in $TiSe_2$, Phys. Rev. Lett. **119**, 176401 (2017).

[40] Y. Tanaka, T. Takeuchi, S. W. Lovesey, K. S. Knight, A. Chainani, T. Takata, M. Oura, Y. Senba, H. Ohashi, and S. Shin, Right Handed or Left Handed? Forbidden x-ray Diffraction Reveals Chirality, Phys. Rev. Lett. **100**, 145502 (2008).

[41] Y. Tanaka, S. P. Collins, S. W. Lovesey, M. Matsunami, T. Moriwaki, and S. Shin, Determination of the absolute chirality of tellurium using resonant diffraction with circularly polarized x-rays, J. Phys.: Condens. Matter **22**, 122201 (2010).

[42] Y. Tanaka, T. Kojima, Y. Takata, A. Chainani, S. W. Lovesey, K. S. Knight, T. Takeuchi, M. Oura, Y. Senba, H. Ohashi, and S. Shin, Determination of structural chirality of berlinite and quartz using resonant x-ray diffraction with circularly polarized x-rays, Phys. Rev. B **81**, 144104 (2010).

[43] K. Momma and F. Izumi, VESTA 3 for three-dimensional visualization of crystal, volumetric and morphology data, J. Appl. Cryst. **44**, 1272 (2011).

[44] O. Bunău and Y. Joly, Self-consistent aspects of x-ray absorption calculations, J. Phys.: Condens. Matter **21**, 345501 (2009).

[45] H. Ueda, M. Porer, J. R. L. Mardegan, S. Parchenko, N. Gurung, F. Fabrizi, M. Ramakrishnan, L. Boie, M. J. Neugebauer, B. Burganov, M. Burian, S. L. Johnson, K. Rossnagel, and U. Staub, Correlation between electronic and structural orders in 1T-$TiSe_2$, Mater. Cloud Arch. **2021**, 48 (2021).